IEEE Access
Multidisciplinary | Rapid Review | Open Access Journal

Received November 30, 2016, accepted January 7, 2017, date of publication February 8, 2017, date of current version March 13, 2017.

Digital Object Identifier 10.1109/ACCESS.2017.2666299

Far-Field RF Wireless Power Transfer with Blind Adaptive Beamforming for Internet of Things Devices

PAVAN S. YEDAVALLI[1, 2], (Student Member, IEEE), TANELI RIIHONEN[3], (Member, IEEE), XIAODONG WANG[1], (Fellow, IEEE), AND JAN M. RABAEY[2], (Fellow, IEEE)

[1]Department of Electrical Engineering, Columbia University, New York City, NY 10027, USA
[2]Department of Electrical Engineering and Computer Sciences, University of California, Berkeley, CA 94720, USA
[3]Department of Signal Processing and Acoustics, Aalto University School of Electrical Engineering, Helsinki, Finland

Corresponding author: T. Riihonen (taneli.riihonen@aalto.fi)

This work was supported in part by Verizon through NYC Media Laboratory, in part by the Peacock Program of Shenzhen under Grant KQTD2015071715073798, and in part by the Leading Talents Program of Guangdong Province under Grant 00201510.

ABSTRACT Wireless power transfer (WPT) has long been one of the main goals of Nikola Tesla, the forefather of electromagnetic applications. In this paper, we investigate radio-frequency beamforming in the radiative far field for WPT. First, an analytical model of the channel fading is presented, and a blind adaptive beamforming algorithm is adapted to the WPT context. The algorithm is computationally light, because we need not explicitly estimate the channel state information. Then, a testbed with a multiple-antenna software-defined radio configuration on the transmitting side and a programmable energy harvester on the receiving side is developed in order to validate the algorithm in this specific power application. From the results, it can be seen that the implementation of this version of beamforming indeed improves the harvested power. Specifically, at various distances from 50 cm to 1.5 m, the algorithm converges with two, three, and four antennas with an increasing gain as we increase the number of antennas. These encouraging results could have far-reaching consequences in providing wireless power to Internet of Things devices, our target application.

INDEX TERMS Wireless power transfer, radio-frequency energy harvesting, software-defined radios, experiments, beamforming.

NOMENCLATURE

BABF	Blind-Adaptive Beamforming
CPU	Central Processing Unit
CW	Continuous Waveform
DC	Direct Current
EGC	Equal Gain Combining
EM	Electromagnetic
FPGA	Field Programmable Gate Array
IoT	Internet of Things
MIMO	Multiple-Input Multiple-Output
MISO	Multiple-Input Single-Output
MR	Magnetic Resonance
MRC	Maximal Ratio Combining
PA	Power Amplifier
PLL	Phase-Locked Loop
PPS	Pulses per Second
RF	Radio Frequency
RSSI	Received Signal Strength Indicator
SMA	SubMiniature Version A
USRP	Universal Software Radio Peripheral
WPT	Wireless Power Transfer

I. INTRODUCTION

Wireless power transfer (WPT) is undoubtedly a concept of the future, but compared to most technologies, it has had a long history, beginning in 1899 with renowned scientist Nikola Tesla. While he was able to show a preliminary proof-of-concept of power being transferred wirelessly, it was not at a level meaningful or safe enough to power any real devices [1]. Today, an encouraging trend is emerging, as there are many academic and industry experts attempting to improve wireless power transfer efficiencies to usable levels. In particular, there are two prevailing approaches of WPT: (a) non-radiative near-field coupling, and (b) far-field RF radiation.

Under the umbrella of non-radiative near-field coupling, there are two different techniques: (a) inductive coupling,

and (b) magnetic resonance coupling. Since all of the magnetic and electric field generation happens in the reactive near field, propagation is minimal due to the power attenuating at $1/d^3$, where d is the distance between the transmitter and receiver [2]. The first approach, inductive coupling, allows for energy to transfer between a transmit and receive coil. The industry standard Qi protocol adopts inductive coupling and specifies ranges up to 40 mm, e.g., see [3]. Researchers in the 'MagMIMO' project are also looking to expand this range further and to use multiple devices [4], [5].

In the second approach of non-radiative near-field coupling, magnetic resonance (MR) coupling, the two coils are now tuned to a resonant frequency, which increases transfer efficiency. 'WiTricity' has looked into systems using MR [2], [6], and Smith *et al.* sought to develop efficient prototypes [7] with magnetic resonance. The industry standard A4WP has also adopted MR as its main technology for WPT [8]. In a slightly different application of WPT, Poon *et al.* have investigated a variation of WPT known as ''mid-field powering'' for deep-tissue implantable devices [9]. However, near-field techniques do not scale well in an Internet of Things (IoT) architecture, where we hope to have devices receive power across wide indoor and outdoor environments.

Thus, we turn our attention to the radiative far field, a more viable alternative to produce longer distance wireless power transfer, on the order of meters. Under this umbrella, there are two approaches: (a) non-directive RF, and (b) directive beamforming. Arbabian *et al.* have explored a system level analysis of RF power delivery at mmWave frequencies using non-directive RF [10]. Another interesting application of non-directive RF is to use ambient radio waves to power devices, specifically from cellular or WiFi. Smith *et al.* developed the 'PoWiFi' testbed using extremely efficient RF-to-direct current (DC) rectifiers [11], but this does not help to solve the still-limiting propagation inefficiency of $1/d^2$ in the far field [12].

The other approach in far-field RF, and one method to overcome free-space path loss, is directive beamforming. Beamforming has been widely adopted as one of the future 5G technologies for data communication [13]. Conceptually, beamforming manipulates each antenna's transmission such that all of them constructively interfere at the receiver. It can be used to overcome propagation loss by directing the radiation exactly to the desired receiver while nulling adjacent interference.

Zhang *et al.* investigated RF beamforming for wirelessly powered communication networks, in which there is a joint design of downlink power transfer and uplink information transfer [14]. Ahn created an implementation of rough RF beamforming at 5.8 GHz using analog phased arrays in hardware. The group hopes for applications in such projects as Google Loon [15], but the prototype requires extensive hardware implementation and provides only coarse beamforming. As it stands, there have neither been theoretical frameworks nor practical prototype implementations of digital beamforming for WPT in academia.

The objective of this paper is to explore the use of digital beamforming for far-field WPT. We consider a lightweight beamforming algorithm that does not require explicit channel estimation, and proceed to investigate the algorithm's effect in maximizing the harvested power. We then empirically validate the analytical results with a novel prototype implementation of the multi-antenna transmitter using software-defined radios and a receiver with an efficient RF energy harvester.

The rest of this paper is structured as follows. An analytical fading model for the adaptive beamforming scheme as well as a theoretical framework are discussed and validated in Section II. The detailed hardware configuration of the experimental testbed is described in Section III. The measurement results are presented and analyzed in Section IV. Finally, Section V concludes the paper.

II. BLIND ADAPTIVE BEAMFORMING

With transmit beamforming, the considered signal model can be expressed as follows:

$$y = \sqrt{G}\,\mathbf{h}^H \mathbf{w}\, x \tag{1}$$

where x is the transmitted signal, $\mathbf{h}$ is the complex channel coefficient vector, and $\mathbf{w}$ is the complex beamforming weight vector, all of dimension N that denotes the number of transmit antennas. The parameter G is the overall gain of the channel, taking into account the antenna gains at both the transmitter and receiver, as well as the general free-space path loss determined by the operation frequency and propagation distance.

Given the context of wireless power transfer, the received signal strength indicator (RSSI) pertaining to the signal y at the harvester is computed as follows:

$$RSSI = G\,|\mathbf{h}^H \mathbf{w}|^2\, P_x, \tag{2}$$

where P_x is the power of the transmitted signal.

Our goal is to maximize the RSSI in the above equation. Theoretically, the optimal weights to maximize received power are equivalent to the typical matched filter in communications that maximizes the signal-to-noise ratio subject to $\|\mathbf{w}\|^2 = N$:

$$\mathbf{w}_{mf} = \sqrt{N} \cdot \frac{\mathbf{h}}{\|\mathbf{h}\|}. \tag{3}$$

With the matched filter, the resulting RSSI is given by

$$RSSI_{mf} = N \cdot G\,\|\mathbf{h}\|^2\, P_x. \tag{4}$$

One should note that we adopt herein the somewhat unconventional normalization whereby the total transmit power of the system is directly proportional to the number of transmit antennas rather than a constant. This is because the operation of our testbed heavily suffers from the low maximum output power of the software-defined radios in use, and thus we need to broadcast all available energy in order to measure

reliable (if any) RSSI values at longer distances. Nevertheless, the experimental results still reveal the true relative gain of adaptive beamforming compared to random beamforming that adopts the same normalization if we keep in mind that there is the absolute gain of $10\log_{10}(N)$ decibels in both due to the unconventional transmit power scaling.

We observe from our experiments that Nakagami-m fading models accurately each element of $\mathbf{h}$, i.e., h_n for $n = 1, 2, \ldots, N$. Thus, RSSI in a single-antenna configuration, $RSSI|_{N=1} = G\,|h_n|^2\,P_x$, is approximately a Gamma random variable with parameters m (shape) and θ (scale). We denote $RSSI|_{N=1} \sim \text{Gamma}(m, \theta)$ and estimate specific values for m and θ from the measurement data, i.e., $m \approx 23$ and $\theta \approx 0.11$ mW when the distance between the transmit antennas and the harvester is 50 cm and average RSSI is $m\theta \approx 2.6$ mW. Unfortunately, the single-antenna setup does not yield enough power with larger distances to get any readings.

For analytical purposes, let us further assume that all elements of $\mathbf{h}$, i.e., h_n for $n = 1, 2, \ldots, N$, are independent and identically distributed (i.i.d.). This is not only because the analysis becomes cumbersome otherwise but also because our measurement data are not statistically suitable for characterizing potential imbalance or correlation in the first place.

The matched filter in (3) combines the channel branches coherently such that the total resulting $RSSI_{mf}$ in (4) is a sum of respective values of $RSSI|_{N=1} = G\,|h_n|^2\,P_x$, $n = 1, 2, \ldots, N$, achieved by each branch alone. Furthermore, it is common knowledge that the sum of i.i.d. Gamma random variables is still a Gamma random variable. Thus, we may denote that $RSSI_{mf} \sim \text{Gamma}(mN, \theta N)$ when using the matched filter (3). The corresponding cumulative distribution function (CDF) of RSSI is given by

$$P\left(RSSI_{mf} < x\right) = 1 - \frac{\Gamma\left(mN, \frac{x}{\theta N}\right)}{\Gamma(mN)}, \tag{5}$$

where $\Gamma(\cdot)$ and $\Gamma(\cdot, \cdot)$ are the Gamma function and upper incomplete Gamma function, respectively. The average and variance of RSSI are given by $\mathrm{E}\left[RSSI_{mf}\right] = mN^2\theta$ and $\mathrm{Var}\left[RSSI_{mf}\right] = mN^3\theta^2$, respectively.

Since the transmitter does not explicitly know the channel, $\mathbf{w}_{mf}$ cannot be used in practice in our experiments. In fact, even the harvester cannot estimate the channel well because it only feeds back RSSI values. Thus, we now discuss a practical solution called blind-adaptive beamforming (BABF), which learns channel characteristics by optimizing $\mathbf{w}$ iteratively [16] such that it also avoids the computational complexity associated with explicit channel estimation. Its performance is superior to random beamforming or equal gain combining (EGC), and approaches that of optimal beamforming (in which $\mathbf{h}$ is explicitly estimated) after a number of iterations [16]. In our experiments, the weights converge over a finite number of iterations, which is a reasonable tradeoff to make for a wireless power transfer application, since latency is not as significant a concern as it is in data communication.

BABF will attempt to converge to the matched filter, essentially mimicking maximal ratio combining (MRC) over a number of iterations. Note that the performance of (3) cannot be fully achieved in reality even with MRC. In particular, redistributing the power budget across separate transmitters does not practically hold because it requires violating the strict per-antenna power constraints which may be impossible if an antenna is already transmitting at the maximum power like in our experiments. Thus, BABF manipulates both the amplitude and phase while the reference case of EGC assumes weights of unit magnitude and optimizes the phases only, which leads to poorer performance.

In our BABF implementation, an initial beamforming weight vector is randomly generated. Then, a continuous wave of constant amplitude and frequency is sent from each transmit antenna, with this weight vector applied to the signal. The receiver then measures the power of the received signal, and feeds back that small packet of information to the transmitter in the form of RSSI. After repeating this process and comparing the received power of each weight vector for that iteration, the index of the weight vector that produces the maximum received power is fed into the blind-adaptive algorithm to determine the next best set of weights. These weights sharpen over a number of iterations to produce the highest received signal within a specified threshold.

Algorithm 1 BABF for Wireless Power Transfer [16]

Initialize $i = 0$ and $w_M^{[0]} \sim \mathcal{N}(0, I)$
while *flag* **do**
  $i \Leftarrow i + 1$
  Generate K perturbation vectors of dimension N, $p_k \sim \mathcal{CN}(0, I)$, $k = 1, ..., K$
  Form K weight vectors, $w_k^{[i]} \Leftarrow \sqrt{N} \cdot \frac{w_M^{[i-1]} + \beta p_k}{||w_M^{[i-1]} + \beta p_k||}$
  for $k = 1$ *to* K **do**
    Measure $RSSI_k^{[i]} = G\left|\mathbf{h}^H \mathbf{w}_k^{[i]}\right|^2 P_x$ at the harvester and feed it back to transmitter
  end
  Determine $M = \text{argmax}_k RSSI_k^{[i]}$
  if $(RSSI_M^{[i]} - RSSI_M^{[i-1]}) < \epsilon$ **then**
    flag = False
  end
end

Algorithm 1 highlights the pseudocode for the implementation of BABF in the context of wireless power transfer, as adapted from [16]. Specifically, at the ith iteration, we will generate the best weight vector $w_M^{[i-1]}$ from the $(i-1)$th iteration, where $M = \text{argmax}_{k=1,2,\ldots,K} RSSI_k$, out of a total of K perturbation vectors. Then, this vector is adjusted by K new random perturbation vectors, whose distributions are normal and complex, $p_k \sim \mathcal{CN}(0, I)$, thus forming K new weight vectors:

$$w_k^{[i]} = \sqrt{N} \cdot \frac{w_M^{[i-1]} + \beta p_k}{||w_M^{[i-1]} + \beta p_k||}, \tag{6}$$

where $k = 1, \ldots, K$. The perturbation factor β affects the weights by adjusting the amplitude and phase of each antenna element, but the entire weight vector is normalized to have unit norm. We empirically choose $K = 10$ and $\beta = 0.2$ for the experiments in our prototype system.

Having established an analytical framework for computing practical beamforming weights in a WPT application, the next task is to verify these results in a real-world system. In the next section, we develop the physical implementation of the pseudocode above in a MISO experimental testbed using software-defined radios and an off-the-shelf energy harvester.

III. HARDWARE CONFIGURATION

A major impediment to powering IoT devices using beamforming is the practical realization of the algorithms. In this paper, considerable effort is spent to discover methods in implementing such algorithms. Toward that objective, this section highlights the importance of the hardware configuration necessary to transmit EM energy wirelessly from multiple antennas to an energy harvester. While accounts of successful implementation were developed using RFID backscattering [16], no efforts have been made with WPT as the objective or with a testbed greater than two antennas. In contrast to RFIDs, our application requires the use of an energy harvester such that we are able to use an actual power metric as feedback to the transmitters for sharpening of the beamforming weights. Consequently, the developed testbed is entirely different.

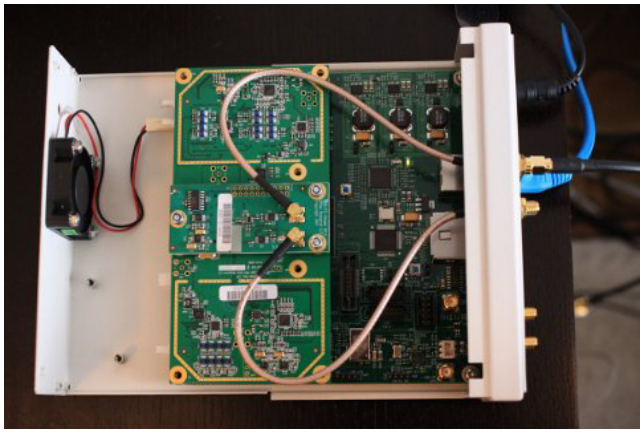

FIGURE 1. USRP N210 transmitter; the setup uses four of these in a planar array to transmit to the energy harvester.

On the transmit side of the configuration, our setup contains four antennas. We use National Instruments Ettus Research USRP N210 units, shown in Figure 1. Each unit is a software-defined radio that contains an FPGA and an RF front end. The signal processing is performed in the FPGA and a connected CPU. Each unit's RF front end is connected to an L-Com 8 dBi flat patch antenna through an SMA connector. These directional antennas are faced toward the receiver, the Powercast P2110 Energy Harvester Evaluation Board Sensor (PS), and are programmed to transmit at an operating frequency of 915 MHz, as constrained by the energy harvester's antenna. The transmit antennas, as a result, are spaced at $\frac{\lambda}{2}$ from one another, making the spacing approximately 17 cm. In addition, each USRP's analog transmit power is at its maximum of 20 dBm, or 100 mW, though BABF ultimately changes the output due to its digital amplitude scaling.

The operation of our testbed is mainly limited at the larger distances by the fact that the maximum USRP transmit power is rather low while the PS only powers up if it receives at least -12 dBm (i.e., approximately 63 μW) of power from RF radiation after conversion to DC. Then, the PS uses a 2.4 GHz antenna operating under the Zigbee protocol to send the RSSI value to the Powercast Receiver (PR). The general flow between the transmitters and receiver is depicted in Figure 2. Note that the off-the-shelf PS has an RF to DC conversion efficiency of 45% to 50% at 915 MHz.

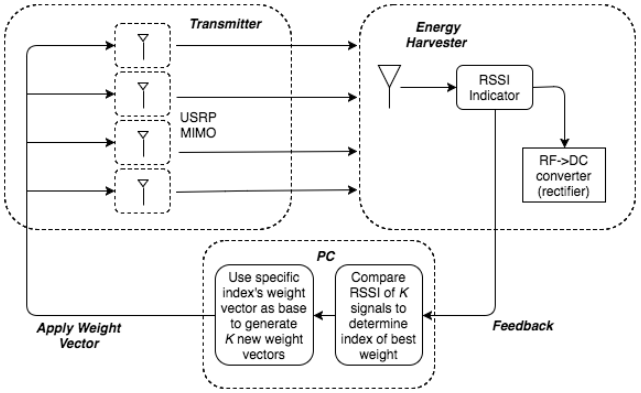

FIGURE 2. Flow with four antennas: Each USRP transmits K signals, each with a weight vector applied, and then the energy harvester collects the RSSI of the combined signals. In practice, the system then feeds back all RSSI values to the PC for comparison in order to determine the index of the weight vector that produces the largest RSSI. Finally, this index is fed into the BABF algorithm to sharpen the weights for the next iteration.

The USRP units (see Fig. 1) run real-time code developed in Python and GNURadio, initially connected to a Lenovo X1 Carbon laptop and then later to a Dell Powerbench desktop (the transition is explained shortly). Since we require feedback from the energy harvester, a novel method that we devised is to connect the PR directly to the desktop via USB using minicom, a modem control and terminal emulation program for UNIX-based operating systems. The RSSI data are fed back from the energy harvester to the PC (which is connected to the transmit USRPs). We then use Python code to parse the RSSI data coming from the PR in order to determine the index of the weight vector (out of K weight vectors) that produces the largest RSSI. This index is then fed into the BABF algorithm to produce new beamforming weights for each antenna, which are then programmed into the FPGAs of the four USRP units. When we order the USRPs to transmit CW tones, these signals are multiplied by the beamforming weights loaded into memory,

and then transmitted out of the antennas toward the energy harvester.

Initially, it was discovered that there was a considerable amount of variation at the RSSI circuit on the energy harvester. Since the channel was generally static in the lab, this variation was coming from the transmitter, receiver, or both. RSSI circuits are generally imprecise, and after much investigation, we soldered a 1 μF smoothing capacitor on the RSSI pin of the circuit board. This decreased the variation to a reasonable level in which the same signal was producing the same received power to the nearest hundredth of a milliwatt, assuming a constant distance and environment.

Another underlying issue was the intermittence of the signal transmission that was causing unpredictable RSSI readings. This was not discovered until an investigation using a Keysight E4440A PSA spectrum analyzer displayed the single tone at 915 MHz frequently disappearing over multiple transmissions. A phenomenon existed in which underflows led to samples from the CPU not arriving at the USRPs for transmission quickly enough. This occurred for two reasons: (a) the 10/100-gigabit Ethernet connection between the CPU and USRPs was not sufficient to transmit a large number of samples across multiple USRPs at a reasonable rate, and (b) the speed of the CPU was not quick enough to manage the number of samples being requested by GNURadio. For these reasons, we were forced to switch from using a laptop configuration to a more powerful desktop configuration with dedicated Ethernet switches, as otherwise too many samples were inundating the CPU and not reaching all the four USRPs.

The speed of the code was also a challenging aspect. GNURadio out-of-tree module blocks were developed in both Python and C++. While in this testbed the Python blocks were implemented, they are slower than those created in C++ because Python code is interpreted at runtime while C++ code is compiled to native code at compile time. This means that the extensibility to even more antennas may require the C++ blocks moving forward.

In addition to the above requirements, a necessity for multi-antenna beamforming systems is that time and frequency synchronization need to be achieved so that each unit is phase-aligned with one another. In order to do this, we connect using SMA cables each USRP's reference clock and PPS signal to the National Instruments Octoclock-G device. The Octoclock-G is a high-accuracy timing and distribution system, so all transmit units have a common clock, as shown in the four antenna setup in Fig. 4. The 10 MHz and PPS outputs of the Octoclock-G were tested using a Tektronix MSO 2024 Mixed Signal Oscilloscope, as displayed in Figure 3. While typically these signals are square waves, jagged artifacts exist because the oscilloscope is not impedance matched to the Octoclock-G.

In initial testing, there existed a random phase offset at each initialization of the USRPs, which occurred at each trial of the algorithm. After programming two USRPs as receivers and using GNURadio timed commands, it was realized that this

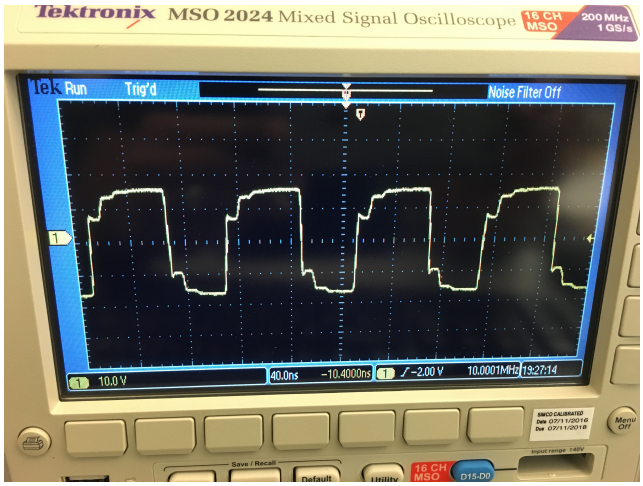

FIGURE 3. Output of Octoclock-G 10 MHz signal to each USRP to determine the alignment of each transmit USRP's clock.

behavior happened due to the default fractional-N PLL of the USRPs. As a result, the code required refactoring to program the boards to perform the tuning of the local oscillator to the proper RF frequency using integer-N PLL.

Finally, given the planar structure of our transmit array, we require that the harvester be positioned at a distance greater than or equal to 49 cm from the transmit structure, as that ensures that it will be in the far-field Fraunhofer region of the antenna aperture. As a result, no unpredictable behavior like Fresnel diffraction is expected. As depicted in Fig. 4, the antennas were placed onto an insulating wooden board using nonconductive tape and oriented vertically so that the harvester's positioning could be systematically adjusted on the lab bench.

IV. MEASUREMENTS AND RESULTS

Having successfully devised a way to measure the received signal power at the energy harvester and collect it back at the transmitter, we now present and discuss the results obtained in the practical implementation of the BABF algorithm for WPT.

Given a pre-determined $\epsilon = 0.001$ and an empirically determined $\beta = 0.2$, we show that the BABF algorithm converges for two, three, and four antenna configurations, and it produces greater received power gains as we increase the number of antennas. While the value of β is originally 0.2, we lower it to 0.02 once the algorithm reaches a steady-state received power, as verification of the stability of the platform. The number of samples collected for each configuration varied based on the sensitivity of the harvester, the interference patterns of the antenna transmissions, and the number of antennas active.

In Fig. 5, the average RSSI is plotted over the number of iterations for the following cases at all four antenna configurations: (a) 50 cm with BABF weights, (b) 100 cm with BABF weights, (c) 50 cm with EGC weights, (d) 100 cm with EGC weights, (e) 50 cm with random weights, and

FIGURE 4. The system setup with four transmit antennas and energy harvester at 100 cm distance.

(f) 100 cm with random weights. Figure 5(e) shows that with random weights, the general pattern of RSSI over a number of iterations is unpredictable but hovers around the same level, averaged over a number of trials.

Contrasting the above with Fig. 5(a), in which we run the same antenna configurations but with the BABF algorithm, we can see not only increased gains over a number of iterations but also the convergence to a greater specified value for each antenna setup. Relative to equal gain combining in Fig. 5(c), the BABF algorithm produces higher RSSI, as it converges to the optimal matched filter. In addition, the consistency of the harvester's getting a sufficient signal was significantly higher with BABF, as out of 65 attempted trials with four and three antenna configurations, we collected 60 each, and out of 20 attempted trials with two antennas, 19 were collected.

The harvester was then moved further away from the transmitters to 100 cm, and similar results were obtained. Naturally at a longer distance, the received power was lower, even with BABF, but the algorithm was able to increase the received power and converge to specific values around 30 iterations, as shown in Fig. 5(b). BABF expectedly performed better than EGC as well, and both expectedly showed drastic improvement compared to random weights. Accordingly for random weights, in Fig. 5(f), the received power for all four antenna configurations stayed relatively constant, with some unpredictable variations, but only a limited number of samples were able to be obtained due to the difficulty for the harvester to receive a sufficient signal. Out of 150 trials with random beamforming, only 75 trials were completed with four antennas, 20 with three antennas, and only 3 with two antennas, suggesting that the distance was much more of a factor than interference at 100 cm. However, with BABF, 100% were successfully obtained with four and three antenna configurations, and 80% with two antennas. This yield varies depending on the amount of time allotted to collect data and the nature of the random weights selected, but theoretically the yield should monotonically decrease with the number of antennas. Using random weights for a single antenna, the power was not sufficient to collect any data, hence its absence in Fig. 5(f). In general, not only are the gains greater with BABF in various antenna configurations, but also there is greater consistency in obtaining any energy, an important component of WPT.

Plotting the empirical cumulative distribution function (CDF) of RSSI values over all iterations and trials in each configuration, we can see in Figs. 6(a) and 6(b) that increasing the number of antennas using BABF contributes to a greater received power at the harvester. The β perturbation value determines how different the random weight vectors are from the base vector (the larger the β, the greater the possible discrepancy from the base vector's performance). An empirically-derived β value of .2 was used, and then it was decreased to $\beta = .02$ after a steady-state RSSI value was noticed. The left tails of the CDFs indicate the nature of this convergence, as the algorithm comes to a level close to the final convergence level quickly (steady-state RSSI value), and then hovers around that level for the bulk of iterations, which makes sense given the smaller β value and thus the smaller variation from the base vector. This left tail behavior exists for EGC in Figs. 6(c) and 6(d) as well. Figs. 6(e) and 6(f) display the extremely low received power at 50 cm and 100 cm, respectively, when using random weights; the coarseness of the plots reflects the lower number of available samples for these configurations.

Based on the single-antenna data collected at a harvester distance of 50 cm, illustrated in Figs. 6(a) and 6(b), we can estimate and model the statistics of the channel branches. In particular, we have $\mathrm{E}[RSSI_1] \approx 2.56$ mW and $\mathrm{Var}[RSSI_1] \approx 0.286$ mW^2 so that basic moment matching yields $m = (\mathrm{E}[RSSI_1])^2/\mathrm{Var}[RSSI_1] \approx 22.82$ when we assume that the channel branch follows Nakagami-m fading. As shown in Fig. 6(a), the analytical CDF plotted as per (5) for the single-antenna setup matches well with the empirical CDF plotted from measurement data.

In multi-antenna configurations, the practical gain achieved with BABF is significantly less than what is predicted by the ideal case with the matched filter. From Figs. 6(a) and 6(b), we can see that the mean initial power tends to increase, marginally with up to three antennas and up to 3 mW with four antennas. However, it appears that the

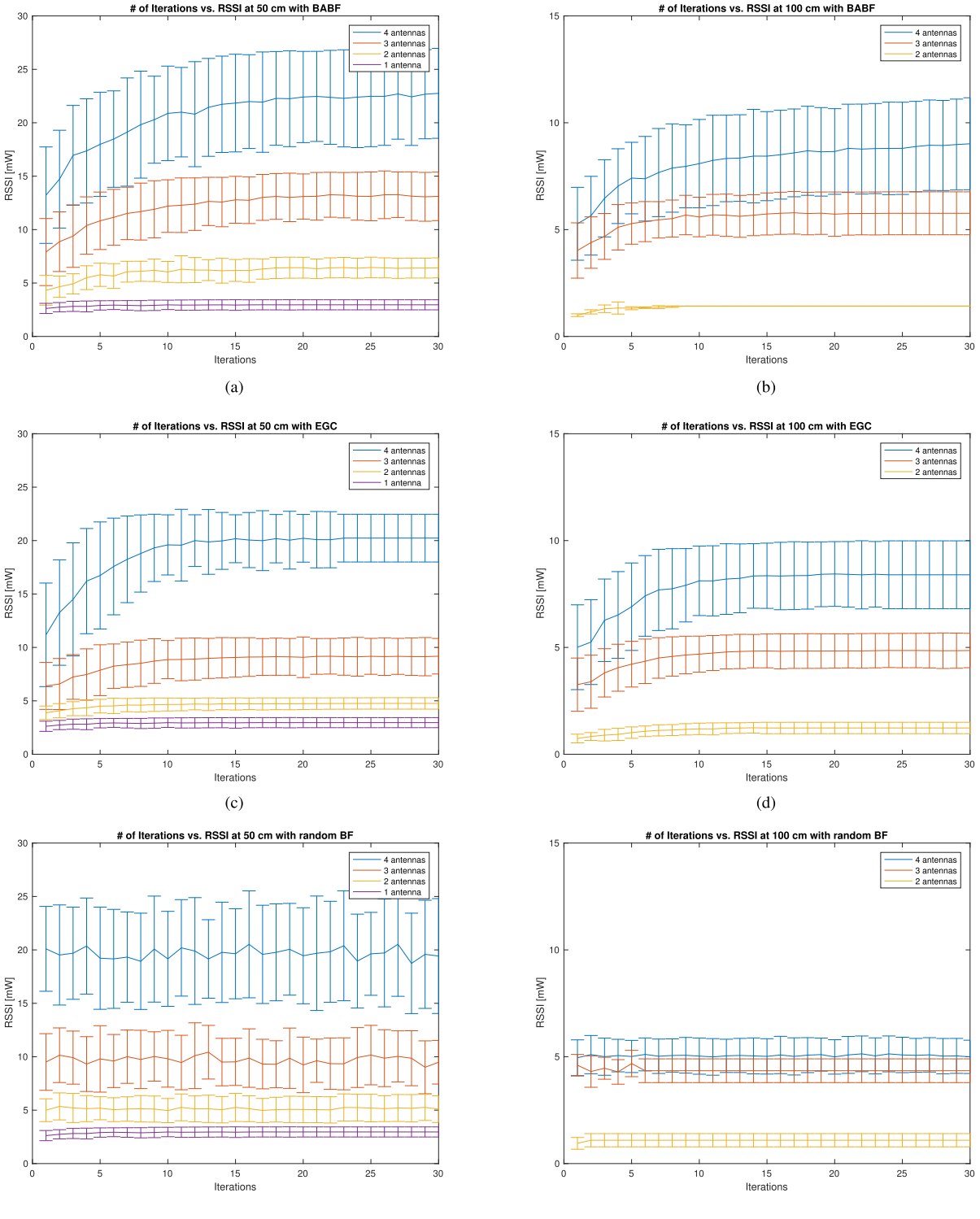

FIGURE 5. The convergence of RSSI gain with BABF, EGC, and random weights at 50 cm (1–4 antennas) and 100 cm (2–4 antennas). The error bars indicate the standard deviation around the average RSSI values. (a) Beamforming with BABF, harvester at 50 cm. (b) Beamforming with BABF, harvester at 100 cm. (c) Beamforming with EGC, harvester at 50 cm. (d) Beamforming with EGC, harvester at 100 cm. (e) Beamforming with random weights, harvester at 50 cm. (f) Beamforming with random weights, harvester at 100 cm.

gain does not scale as expected with $10\log_{10}(2) = 3$ dB and $10\log_{10}(4) = 6$ dB, suggesting there could be other parameters at play. The maximum theoretical distance based on a link budget with $f = 915$ MHz, $P_t = 20$ dBm, $G_{tx} = 8$ dBi, $G_{rx} = 0$ dBi, and the aforementioned maximum array gain of 6 dB with a minimum received power

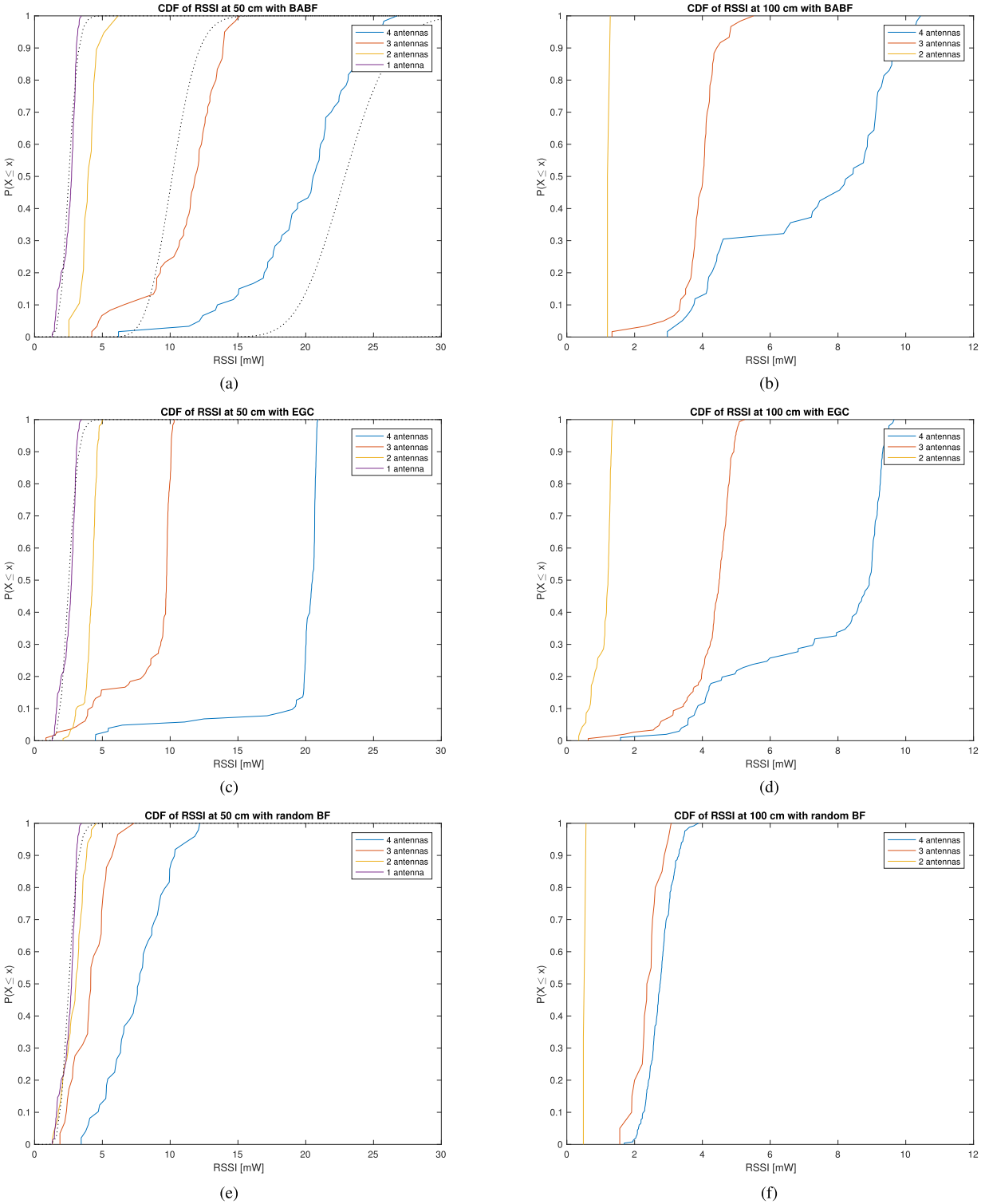

FIGURE 6. Cumulative distribution function of RSSI with BABF, EGC, and random weights at 50 cm (1–4 antennas) and 100 cm (2–4 antennas). (a) Beamforming with BABF, harvester at 50 cm. (b) Beamforming with BABF, harvester at 100 cm. (c) Beamforming with EGC, harvester at 50 cm. (d) Beamforming with EGC, harvester at 100 cm. (e) Beamforming with random weights, harvester at 50 cm. (f) Beamforming with random weights, harvester at 100 cm.

of −12 dBm at the energy harvester, is 5.2 m with three antennas (2.6 m with one antenna). However, our setup does not achieve this distance. One reason could be that since both amplitude and phase weighting are done, analog irregularities in the RF circuit could result from the digital scaling, and since the devices are not frequently calibrated, potential phase

drift among the USRP clocks as well as amplitude distortion could arise. Spurious tones were detected on the spectrum analyzer occasionally as well, which could also limit performance. Another reason is that the power amplifier (PA) efficiency may also be lower than in the optimal operating regime. This is a function of temperature and frequency, as well as intrinsic device characteristics of the PA [17], which were not optimized in this testbed. This may lead to less power available at the input of the transmit antenna.

It is no surprise that BABF yields better RSSI than EGC because the former is allowed to violate the per-antenna power constraint. EGC does not allow for dynamic power allocation to antennas with good channels, as BABF does. This effect, as we can see, is more pronounced with more antennas. Typically, in multi-antenna systems, the total power is kept as a constant. In this scenario, we scaled by the number of antennas for BABF, and transmitted the maximum power from each antenna for EGC. Since BABF distributes the power across the antennas more optimally, it performs better than EGC, while both of course perform much better than random weights.

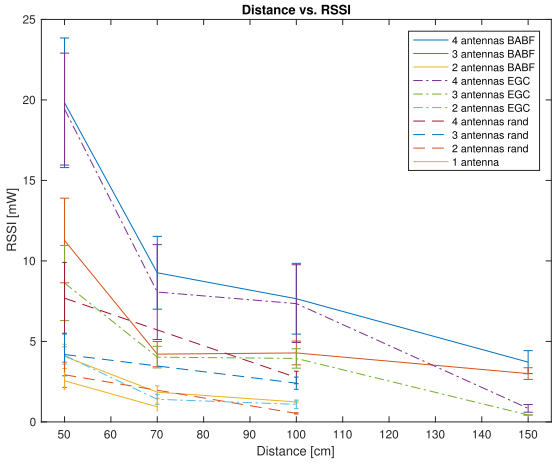

FIGURE 7. Average RSSI compared to distance with BABF, EGC, and random weights. The number of antennas for each type of weight varies from 1 to 4, and the distances vary between 50 cm and 150 cm, depending on the type of weight.

Figure 7 shows a curve of best fit between average RSSI and distance in different antenna and weighting configurations. Having collected data at 50 cm, 70 cm, 100 cm, and 150 cm, we see, unsurprisingly, that the greatest gains occur at the shortest distances as we increase the number of antennas. The relationship generally follows the $1/d^2$ inverse square law behavior of free space path loss, but we can see greater gains using BABF. The random weights clearly cannot compete with the BABF weights in producing higher RSSI. No data could be collected with random weights at a distance greater than 50 cm with a single antenna or at distances greater than 100 cm with two-to-four antennas. In addition, the number of data points at a distance of 100 cm for two antennas with BABF is small, as shown in Fig. 6(b).

The implementation of the BABF algorithm using an energy harvester clearly shows that as the number of antennas increases, the gain continues to increase over a number of iterations until the algorithm converges. In addition, from Fig. 7, we can see that at greater distances, a greater minimum number of antennas is required to realize the benefits of beamforming in the MISO architecture. In Fig. 7, a range of 50 to 150 cm between the antennas and energy harvester was tested, peaking at 150 cm due to the speed of the data collection becoming exceedingly slow at greater distances. These encouraging results suggest that the algorithm is a suitable choice for extending the setup to more antennas with more optimal software and hardware for practical wireless power transfer applications.

V. CONCLUSION

In this paper, we have presented both an analytical framework as well as a practical implementation for a wireless power transfer (WPT) application using beamforming. The analytical framework describes a lightweight iterative computation of the beamforming weights without costly explicit channel estimation, as well as a channel model. In the practical testbed, we implement this blind adaptive beamforming scheme in a multi-antenna transmit setup using software-defined radios. These radios are aligned such that they have a common clock, and they transmit continuous tones at the same time to the energy harvester, which feeds back to the algorithm the index of the weights that produces the best RSSI signal.

Our encouraging results show that the algorithm substantially improves the received power over a number of iterations at various antenna configurations and distances of up to 1.5 m. Compared to no beamforming at one antenna, random beamforming in two-to-four antenna setups, and equal gain combining in two-to-four antenna setups, blind adaptive beamforming sees the greatest increases. When the range of the system is increased to 1.5 m, it is observed that a higher minimum number of antennas is necessary to realize greater received power, suggesting that if the system is scaled to more antennas, even larger gains and thus longer distances can be achieved.

The present testbed could easily be extended to more antennas, in hopes that eventually a true radio frequency integrated circuit could be developed for WPT. Antenna design, mutual coupling, and software latency will be challenging when developing such a circuit. With many IoT devices, such as implantable sensors, wearable electronics, and motion or temperature sensors - all requiring power on the order of milliwatts, as shown in the testbed-beamformed power over noticeable distances is a reality.

ACKNOWLEDGMENTS

In addition to the funding sources, the authors would like to thank the research staff and resources at Berkeley Wireless Research Center.

REFERENCES

[1] K. Huang and X. Zhou, "Cutting the last wires for mobile communications by microwave power transfer," *IEEE Commun. Mag.*, vol. 53, no. 6, pp. 86–93, Jun. 2015.
[2] X. Lu, P. Wang, D. Niyato, D. I. Kim, and Z. Han, "Wireless charging technologies: Fundamentals, standards, and network applications," *IEEE Commun. Surveys Tuts.*, vol. 18, no. 2, pp. 1413–1452, 2nd Quart., 2016.
[3] S. Y. Hui, "Planar wireless charging technology for portable electronic products and Qi," *Proc. IEEE*, vol. 101, no. 6, pp. 1290–1301, Jun. 2013.
[4] J. Jadidian and D. Katabi, "Magnetic MIMO: How to charge your phone in your pocket," in *Proc. 20th Annu. Int. Conf. Mobile Comput. Netw.*, Sep. 2014, pp. 495–506. [Online]. Available: http://doi.acm.org/10.1145/2639108.2639130
[5] L. Shi, Z. Kabelac, D. Katabi, and D. Perreault, "Wireless power hotspot that charges all of your devices," in *Proc. 21st Annu. Int. Conf. Mobile Comput. Netw.*, 2015, pp. 2–13. [Online]. Available: http://doi.acm.org/10.1145/2789168.2790092
[6] J. Gozalvez, "WiTricity—The wireless power transfer," *IEEE Veh. Technol. Mag.*, vol. 2, no. 2, pp. 38–44, Jun. 2007.
[7] A. P. Sample, B. H. Waters, S. T. Wisdom, and J. R. Smith, "Enabling seamless wireless power delivery in dynamic environments," *Proc. IEEE*, vol. 101, no. 6, pp. 1343–1358, Jun. 2013.
[8] F. Zhang, S. A. Hackworth, W. Fu, and M. Sun, "The relay effect on wireless power transfer using WiTricity," in *Proc. 14th Biennial IEEE Conf. Electromagn. Field Comput. (CEFC)*, May 2010, p. 1.
[9] J. S. Ho *et al.*, "Wireless power transfer to deep-tissue microimplants," *Proc. Nat. Acad. Sci. USA*, vol. 111, no. 22, pp. 7974–7979, Apr. 2014.
[10] J. Charthad, N. Dolatsha, A. Rekhi, and A. Arbabian, "System-level analysis of far-field radio frequency power delivery for mm-sized sensor nodes," *IEEE Trans. Circuits Syst. I, Reg. Papers*, vol. 63, no. 2, pp. 300–311, Feb. 2016.
[11] V. Talla, B. Kellogg, B. Ransford, S. Naderiparizi, S. Gollakota, and J. R. Smith, "Powering the next billion devices with Wi-Fi," in *Proc. 11th ACM Conf. Emerg. Netw. Experim. Technol.*, 2015, pp. 4-1–4-13. [Online]. Available: http://doi.acm.org/10.1145/2716281.2836089
[12] B. Sklar, *Digital Communications: Fundamentals and Applications*. Upper Saddle River, NJ, USA: Prentice-Hall, 1988.
[13] F. W. Vook, A. Ghosh, and T. A. Thomas, "MIMO and beamforming solutions for 5G technology," in *Proc. IEEE MTT-S Int. Microw. Symp.*, Jun. 2014, pp. 1–4.
[14] L. Liu, R. Zhang, and K.-C. Chua, "Multi-antenna wireless powered communication with energy beamforming," *IEEE Trans. Commun.*, vol. 62, no. 12, pp. 4349–4361, Dec. 2014.
[15] C. J. Ahn, "Wireless power transmission with rough beamforming method," in *Proc. 2nd Nat. Found. Sci. Technol. Develop. Conf. Inf. Comput. Sci. (NICS)*, Sep. 2015, pp. 305–309.
[16] S. Chen, S. Zhong, S. Yang, and X. Wang, "A multi-antenna RFID reader with blind adaptive beamforming," *IEEE Internet Things J.*, vol. 3, no. 6, pp. 986–996, Dec. 2016.
[17] D. M. Pozar, *Microwave Engineering*, 4th ed. Hoboken, NJ, USA: Wiley, 2011.

PAVAN S. YEDAVALLI (S'11) received the B.Sc. degree in electrical engineering and computer sciences from the University of California at Berkeley, Berkeley, in 2009, and the M.Sc. degree from Columbia University in electrical engineering in 2011, where he is currently pursuing the Ph.D. degree in electrical engineering. From 2011 to 2015, he was with industry developing multi-antenna beamforming systems for wireless backhaul. He is currently a Visiting Researcher with the Berkeley Wireless Research Center, University of California at Berkeley. His research interests include wireless power transfer, wireless communications, MIMO RF embedded systems, and Internet of Things architectures. He is a recipient of the NYC Media Laboratory and Verizon Open Innovation Group's Connected Futures Research Grant.

TANELI RIIHONEN (M'14) received the D.Sc. degree in electrical engineering (Hons.) from Aalto University, Helsinki, Finland, in 2014. He was a Visiting Associate Research Scientist and an Adjunct Assistant Professor with Columbia University, City of New York, USA, from 2014 to 2015. He has held various research positions with the Department of Signal Processing and Acoustics, Aalto University School of Electrical Engineering, since 2005, being currently appointed as a Research Fellow. His research activity is focused on physical-layer OFDM(A), multiantenna, relaying and full-duplex wireless techniques with current interest in the evolution of 5G systems. He received the Finnish Technical Sector's Award for the best doctoral dissertation of the year in Finland within all engineering sciences. He has been nominated eleven times as an Exemplary/Top Reviewer and the Reviewer of the Month in various IEEE journals, including the IEEE Access, and is an Editor of the IEEE Communications Letters since 2014.

XIAODONG WANG (F'08) received the Ph.D. degree in electrical engineering from Princeton University. He is currently a Professor of Electrical Engineering with Columbia University, New York. His research interests fall in the general areas of computing, signal processing and communications, and has authored extensively in these areas. He has authored the book *Wireless Communication Systems: Advanced Techniques for Signal Reception* (Prentice Hall, 2003). His current research interests include wireless communications, statistical signal processing, and genomic signal processing. He received the 1999 NSF CAREER Award, the 2001 IEEE Communications Society and Information Theory Society Joint Paper Award, and the 2011 IEEE Communication Society Award for Outstanding Paper on New Communication Topics. He has served as an Associate Editor of the IEEE Transactions on Communications, the IEEE Transactions on Wireless Communications, the IEEE Transactions on Signal Processing, and the IEEE Transactions on Information Theory. He is listed as an ISI Highly-cited Author.

JAN M. RABAEY (F'95) received the Ph.D. degree in applied sciences from Katholieke Universiteit Leuven, Leuven, Belgium. He was with the University of California at Berkeley, Berkeley, CA, USA, as a Visiting Research Engineer. He was a Research Manager with IMEC, Leuven. In 1987, he joined the Faculty of the Electrical Engineering and Computer Science Department, University of California at Berkeley, where he holds the Donald O. Pederson Distinguished Professorship. He is currently the Scientific Co-director of the Berkeley Wireless Research Center, and the Director of the FCRP Multiscale Systems Research Center. His research interests include the conception and implementation of next-generation integrated wireless systems. He was a recipient of a wide range of awards, including the 2008 IEEE Circuits and Systems Society Mac Van Valkenburg Award, the 2009 European Design Automation Association Lifetime Achievement Award, and the prestigious Semiconductor Industry Association University Researcher Award in 2010.